COMPARISON OF SINE-WAVE FREQUENCY ESTIMATION METHODS IN RESPECT OF SPEED AND ACCURACY FOR A FEW OBSERVED CYCLES DISTORTED BY NOISE AND HARMONICS

Józef Borkowski, Dariusz Kania, Janusz Mroczka

Wrocław University of Science and Technology, Faculty of Electronics, B. Prusa 53/55, 50-317 Wrocław, Poland
(*Jozef.Borkowski@pwr.edu.pl,* ✉ *Dariusz.Kania@pwr.edu.pl,* +48 71 320 6329, *Janusz.Mroczka@pwr.edu.pl*)

Abstract

The paper deals with frequency estimation methods of sine-wave signals for a few signal cycles and consists of two parts. The first part contains a short overview where analytical error formulae for a signal distorted by noise and harmonics are presented. These formulae are compared with other accurate equations presented previously by the authors which are even more accurate below one cycle in the measurement window. The second part contains a comparison of eight estimation methods (ESPRIT, TLS, Prony LS, a newly developed IpDFT method and four other 3-point IpDFT methods) in respect of calculation time and accuracy for an ideal sine-wave signal, signal distorted by AWGN noise and a signal distorted by harmonics. The number of signal cycles is limited from 0.1 to 3 or 5. The results enable to select the most accurate/ fastest estimation method in various measurement conditions. Parametric methods are more accurate but also much slower than IpDFT methods (up to 3000 times for the number of samples equal to 5000). The presented method is more accurate than other IpDFT methods and much faster than parametric methods, which makes it possible to use it as an alternative, especially in real-time applications.

Keywords: DFT spectrum interpolation, short-time frequency estimation, statistical analysis, Prony LS, TLS, ESPRIT.

1. Introduction

The digital processing of sine-wave signals is the fundamental issue in many areas of science technology and it is employed *e.g.* in telecommunications, acoustics, electronics, analysis of mechanical vibrations, biomedical applications, renewable energy systems [1–6]. Obtaining the signal frequency value is often the primary goal of this processing [7]. In practice, such signals are often distorted by noise and harmonics and their analysis has to meet some speed and accuracy requirements. The basic estimation methods are basically divided regarding the calculation domain. Methods in the time domain are based on analysis of consecutive signal values, whereas methods in the frequency domain are based on analysis of various signal spectrum estimators. The second domain is often used mainly because of better accuracy of the provided results. In this paper also another division (parametric and nonparametric methods can be here distinguished) of estimation methods is used in respect of the initial signal model assumptions

and the way of calculation of the parameters [8–13]. The main advantage of the first group is its very good accuracy. However, these methods are also computationally complex, so that there is necessary to select an appropriate model order. Moreover, they are often hard to implement in real-time systems. In this group there are *e.g.* subspace methods (Pisarenko, MUSIC – *Multiple Signal Classification*, ESPRIT – *Estimation of Signal Parameters via Rotational Invariance Techniques*, MN – *Minimum Norm*, *etc.*), parametric modelling methods (AR – *Autoregressive*, MA – *Moving Average*, ARMA – *Autoregressive Moving Average*), Prony's method and its modifications, TLS (*Total Least Squares*). The second group contains classical methods of the Fourier analysis where the Fourier resolution is the frequency resolution. In this case, the estimation accuracy is much lower and there at least two or three signal cycles should be analysed to obtain better resolution and acceptable results. Moreover, these methods are not computationally complex and their implementation is straightforward, what makes them still very popular in many real-time applications. Over the last years, some efforts to make complex calculations possibly fast and to improve the estimation accuracy have been made. For example, in some parametric methods the Gohberg–Semencul procedure can be used to solve equations based on the Toeplitz matrix while the spectrum interpolation is widely used to improve accuracy in the Fourier methods [14]. In particular, the spectrum interpolation methods (IpDFT – *Interpolated DFT*) have been very popular in the recent years, as well as MWIDFT (*Multipoint Weighted Interpolation of DFT*) methods where spectrum points around the main lobe are weighted properly in dependence on the method [6, 15–24]. To reduce the spectrum leakage time windows other than the rectangle window are used. Very popular are I class Rife-Vincent (MSD – *Maximum Sidelobe Decay*) windows which belong to the cosine windows. They have very good properties (which can be changed using various values of the window order) in the frequency domain and their spectrum equation has a simple, analytical form which has a great importance in formulating the estimators' equations.

In the recent years, a new IpDFT method has been presented in several papers, *e.g.* [6, 19–22], that include analytical formulas, simulations and experiments in real-time systems using a DSP processor. It is based on the 3-point spectrum interpolation, MSD windows and the Fast Fourier Transform procedure. The method enables to determine frequency of sine-wave signals for observed cycles below two (or even one) which has a great importance in real-time systems. The method is also universal (there are no crucial assumptions on the signal model) and the value can be determined in a non-iterative way. It offers a very good accuracy and calculation speed because of using the FFT transform. Recently, the authors of [23] tried to compare this method to their own. They also presented analytical formulas for errors' equations for a signal distorted by wideband noise and harmonic components. However, they are probably not familiar with the papers [20, 21] from 2015 and 2016, where there were presented the *MSE* error as well as the error equation in the presence of harmonic components.

There are not many papers dealing with comparison of estimation methods regarding their accuracy and calculation speed. In [10] the authors compare a method based on the DFT and the MUSIC method in respect of estimation speed in medical applications. The authors of [25] compare the AR and DFT-based methods in respect of their accuracy. The more signals were distorted by noise the more the DFT-based method was preferred and vice versa. The main conclusions from it can be found in [26] and [27], where a method based on the FFT and the Prony's method were compared and the second was more accurate in the case of harmonic components being present in an analysed signal. In this paper eight (Prony LS, TLS, ESPRIT and five 3-point IpDFT methods) estimation methods are compared in respect of both their estimation accuracy and estimation speed. The tests were performed for an ideal sine-wave signal, for a signal distorted by AWGN noise and for a signal distorted by harmonic components. The re-

sults enable to select the most accurate/the fastest estimation method in various measurement conditions.

The first part of this paper (Section 2) is dedicated to a short overview of [6] and [23] and comparison of the obtained errors' expressions. In Section 3 eight estimation methods are compared in respect of their accuracy and calculation time. Finally, the conclusions are presented in Section 4 and the derived formula of expression to obtain values of estimation errors for a signal distorted by harmonics can be found in Appendix.

2. Comparison of errors' expressions

The newly presented estimation method was developed for photovoltaic systems where estimation of the grid signal plays a great role in the inverter control and the system efficiency. Moreover, the method is universal and can be used to analyse signals in many other applications, *e.g.* to eliminate mechanical oscillations [20]. The maximum estimation time has to be below two cycles of the grid signal (below 40 ms) because of some requirements, as defined in the respective standards and directives. A sine-wave signal (*e.g.* the grid signal) is a special case of a multi-frequency signal described in the time domain as the sum of M sinusoidal components:

$$x(t) = \sum_{L=1}^{M} A_L \sin(2\pi f_L t + \varphi_L), \tag{1}$$

where f_L is a frequency of L-th component; A_L and φ_L are its amplitude and phase, respectively. In the signal, there can be distinguished the basic component (for $L = 1$) and harmonic components (for $L > 1$ and $f_L = L \times f_1$, where $L = 2, 3, \ldots, M$). The analogue signal $x(t)$ is first sampled with a sampling frequency $f_s = 1/T$ and N samples x_n (for $n = 0, \ldots, N-1$) using the H-order MSD windows are obtained. Later, the spectrum is calculated using the FFT transform and, based on three values X_{k-1}, X_k, X_{k+1}, where k is a spectrum line index, the frequency value is determined in respect of measurement time NT. This normalized value is called λ or *CiR* (*Cycle in Range*) and is equal to $\lambda_L = f_L NT$ [bin]. The method enables to eliminate the impact of the conjugate's component on the estimation's outcome.

The method is based on using the H-order I class Rife-Vincent (MSD) time windows which belong to the cosine windows' family defined as [28–30]:

$$w_n = \sum_{h=0}^{H-1} (-1)^h a_h \cos\left(\frac{2\pi nh}{N}\right), \qquad n = 0, \ldots, N-1, \tag{2}$$

where coefficients H for MSD windows are defined as:

$$a_0 = \frac{C_{2H-2}^{H-1}}{2^{2H-2}},$$
$$a_h = \frac{C_{2H-2}^{H-h-1}}{2^{2H-3}}, \quad h = 1, \ldots, H-1, \tag{3}$$

where

$$C_m^p = \binom{m}{p} = \frac{m!}{(m-p)!p!}. \tag{4}$$

Equation (3) were defined by Belega [31] in a heuristic way and proved that it fulfilled the three conditions defined by Nutall [28]. A direct derivation of (3) from the Rife-Vincent result

[29] is given in [6] based on the normalization condition: $\max_n w_n = 1$. The spectrum for these windows can be approximated for $H > 1$, $N \gg 1$ and $N \gg \lambda$ by [30]:

$$W(\lambda) = \frac{D(\lambda)}{P(\lambda)}, \tag{5}$$

where

$$D(\lambda) = \frac{N(2H-2)!}{\pi 2^{2H-2}} \sin(\pi\lambda) e^{-j\pi\lambda}, \tag{6}$$

$$P(\lambda) = \lambda \prod_{h=1}^{H-1}(h^2 - \lambda^2) = \frac{\prod_{h=0}^{H}(h^2 - \lambda^2)}{(-\lambda)(H-\lambda)(H+\lambda)}. \tag{7}$$

For $H = 1$ and $H = 2$ the spectra of the rectangular and Hanning windows are obtained, respectively. The DFT spectrum of signal x_n is:

$$X(\lambda) = \sum_{n=0}^{N-1} x_n w_n e^{-j2\pi n\lambda/N}. \tag{8}$$

If there is only the basic component in the signal or the spectrum leakage from harmonic components is properly reduced, the spectrum (8) is:

$$X(\lambda) = \frac{A_1}{2j} e^{j\varphi_1} W(\lambda - \lambda_1) - \frac{A_1}{2j} e^{-j\varphi_1} W(\lambda + \lambda_1), \tag{9}$$

where $-\lambda_1$ is a value of frequency for the conjugate component (image component) in the spectrum. Taking into consideration (5), (9) can be expressed as follows:

$$X(\lambda) = \frac{A_1}{2j} e^{j\varphi_1} \frac{D(\lambda - \lambda_1)}{P(\lambda - \lambda_1)} - \frac{A_1}{2j} e^{-j\varphi_1} \frac{D(\lambda + \lambda_1)}{P(\lambda + \lambda_1)}. \tag{10}$$

For three successive spectrum points: X_{k-1}, X_k, X_{k+1} (for $\lambda = k-1$, k, $k+1$), there can be obtained three equations based on which the frequency equation (11) can be calculated [6], what brings to generalization of the equations obtained by Chen [32] for the Hanning window case.

The normalized frequency can be determined as follows [6]:

$$\hat{\lambda}_1 = \mathrm{Re}\left\{\sqrt{\frac{\Pi_1}{\Pi_2}}\right\}, \tag{11}$$

where

$$\Pi_1 = \begin{vmatrix} (2H-1)H & (2H-1) & X_{k-1}-X_k \\ -k^2-H^2 & 2k & X_k \\ (2H-1)H & -(2H-1) & X_{k+1}-X_k \end{vmatrix}, \tag{12}$$

$$\Pi_2 = \begin{vmatrix} 1 & -(2H-1) & X_{k-1} \\ 1 & 0 & X_k \\ 1 & (2H-1) & X_{k+1} \end{vmatrix} = (2H-1)\begin{vmatrix} 1 & X_{k-1}-X_k \\ -1 & X_{k+1}-X_k \end{vmatrix}. \tag{13}$$

In [6], the real part operator Re{.} was omitted due to an oversight in typesetting. In all simulations and experiments presented in [6] this operator was used, what was necessary by the fact that frequency must be real. The frequency (11) can be presented in other forms, *e.g.* as:

$$\hat{\lambda}_1 = \text{Re}\left\{ \sqrt{-\frac{2H\left(X_k+k(X_{k-1}-X_{k+1})\right)+k^2(2X_k-X_{k-1}-X_{k+1})-H^2(2X_k+X_{k-1}+X_{k+1})}{X_{k-1}-2X_k+X_{k+1}}} \right\}. \quad (14)$$

The k value should be appropriately selected to obtain the most accurate results for given measurement parameters. There is no limit for the k value but for the special case when $k = 0$ (12), (13) and (14) are respectively:

$$\Pi_1 = \begin{vmatrix} -(2H-1)H & -(2H-1) & X_{k-1}-X_k \\ H^2 & 0 & X_k \\ -(2H-1)H & (2H-1) & X_{k+1}-X_k \end{vmatrix}, \quad (15)$$

$$\Pi_2 = \begin{vmatrix} 1 & -(2H-1) & X_{k-1} \\ 1 & 0 & X_k \\ 1 & (2H-1) & X_{k+1} \end{vmatrix} = (2H-1)\begin{vmatrix} 1 & X_{k-1}-X_k \\ -1 & X_{k+1}-X_k \end{vmatrix}, \quad (16)$$

$$\hat{\lambda}_1 = \text{Re}\left\{ \sqrt{H\frac{2X_k(H-1)+H(X_{k-1}+X_{k+1})}{X_{k-1}-2X_k+X_{k+1}}} \right\}. \quad (17)$$

Taking into consideration that for $k = 0$:

$$X_{k-1} = X_{k+1}^*, \quad (18)$$

and

$$X_{k-1} + X_{k+1} = 2\text{Re}\{X_{k+1}\}. \quad (19)$$

Equation (17) takes the form:

$$\hat{\lambda}_1 = \text{Re}\left\{ \sqrt{H\frac{X_k(H-1)+H\text{Re}\{X_{k+1}\}}{-X_k+\text{Re}\{X_{k+1}\}}} \right\}. \quad (20)$$

The 3-point interpolation is then a 2-point interpolation which changes the idea of the method.

In [23] the authors try to compare the presented method with their own. One of the main conclusions is that the presented method is more accurate for a very small number of signal cycles (less than 1.5) and faster by about 8%, because the method from [23] is iterative and differs from the method presented in this paper where the frequency value is obtained only in one step. However, in [23] there are some misunderstandings which will be cleared up in this paper. The authors of [23] give an expression for the *MSE* error of the proposed method estimator (when AWGN noise is present in the signal) and an expression for the estimation error caused by harmonics present in the signal. However, the authors do not mention two papers ([20, 21]) in which these expressions were presented in 2015 and 2016. Now, in this part of the paper these expressions will be compared because they differ regarding accuracy.

The total error of the presented method consists of two components:

$$
\max_{\varphi_1,\dots,\varphi_L}|\delta_t\lambda_1| = \overbrace{\max_{\varphi_1}|\delta\lambda_1| + \sum_{L=2}^{M}\max_{\varphi_1,\dots,\varphi_L}|\delta_{h,L}\lambda_1|}^{\text{Systematic component}} + \overbrace{\max_{\varphi_1}|\delta_n\lambda_1|}^{\text{Random component}} .
\tag{21}
$$

The systematic component is associated with the discrete nature of DFT, approximations of equations for the time window spectrum, the non-coherent sampling and the presence of harmonic components in the analysed signal. The random component occurs because of the presence of noise in the signal. Based on several papers, *e.g.* [6, 19–22], it can be written that the signal phase has a big impact on the estimation results. Because of that, the estimation errors are calculated as the maximum values from the whole range of the signal phase (and phases of harmonics).

In practice, the signal (1) is distorted by noise which very often is the sum of noises with various probability distributions. However, based on the central limit theorem it can be assumed that a probability distribution is close to a normal distribution. Because of that, it is worth testing the estimation methods in the presence of AWGN (*Additive White Gaussian Noise*) noise (with variance σ_n^2 and zero mean) in the signal. From a practical point of view, it is good to know the analytical form that enables to calculate the estimation error when the signal is distorted by noise. The error value can be obtained based on the estimator variance (or the standard deviation) as $k_p \cdot \sigma_{\lambda_1}$ where k_p is a coverage factor most often equal to 2 or 3, and σ_{λ_1} is the estimator standard deviation of frequency.

The *MSE* error of the estimator can be calculated to assess its quality. It comprises two components: the estimator variance and the squared bias of this estimator:

$$
MSE\left(\hat{\lambda}_1\right) = Var\left(\hat{\lambda}_1\right) + \left(Bias\left(\hat{\lambda}_1\right)\right)^2.
\tag{22}
$$

The *MSE* without bias is variance. According to the results given in several papers, *e.g.* [6, 19–22], it can be assumed that the second component in (22) is negligibly small in relation to the variance and in this case the *MSE* error and the variance can be used interchangeably in this paper. The analytical form of variance (standard deviation) was presented in 2016 [21] taking into account the conjugate component in the signal spectrum (there were no approximations while determining the equation except those like made in (5)) and it was derived by applying the uncertainty propagation law to (14). In this paper, the expression is improved by eliminating the image part of it, so that no complex value can be obtained:

$$
MSE\left(\hat{\lambda}_1\right) \cong \sigma_{\lambda_1}^2 \cong \left[\frac{2^{2H}}{A\lambda_1\,\mathrm{sinc}\left(\pi(\lambda_1-1)\right)\sqrt{N}(2H-2)}\sigma_n\sqrt{\frac{C_{4H=4}^{2H-2}}{2^{4H-4}}} \right.
$$

$$
\cdot\frac{(1+\lambda_1)\prod\limits_{h=1}^{H}\left(h^2-(1-\lambda_1)^2\right)\prod\limits_{h=1}^{H}\left(h^2-(1+\lambda_1)^2\right)}{(1-\lambda_1)\prod\limits_{h=1}^{H}\left(h^2-(1-\lambda_1)^2\right)+(1+\lambda_1)\prod\limits_{h=1}^{H}\left(h^2-(1+\lambda_1)^2\right)}
\tag{23}
$$

$$
\left.\cdot\sqrt{\frac{3+H(16-2H+22H^2+3H^3)+\lambda_1^2(4H-3)\left(-2(-1+H(4+H))+\lambda_1^2(4H-1)\right)}{64H^3(2H-1)^3}}\right]^2,
$$

which can be also presented using the *SNR* parameter:

$$
\begin{aligned}
MSE\left(\hat{\lambda}_1\right) &\cong \sigma_{\lambda_1}^2 \cong \Bigg[\frac{2^{2H}}{\sqrt{2}SNR\lambda_1 \operatorname{sinc}\left(\pi(\lambda_1-1)\right)\sqrt{N}(2H-2)}\sqrt{\frac{C_{4H=4}^{2H-2}}{2^{4H-4}}} \\
&\quad \cdot \frac{(1+\lambda_1)\prod\limits_{h=1}^{H}\left(h^2-(1-\lambda_1)^2\right)\prod\limits_{h=1}^{H}\left(h^2-(1+\lambda_1)^2\right)}{(1-\lambda_1)\prod\limits_{h=1}^{H}\left(h^2-(1-\lambda_1)^2\right)+(1+\lambda_1)\prod\limits_{h=1}^{H}\left(h^2-(1+\lambda_1)^2\right)} \\
&\quad \cdot \sqrt{\frac{3+H(16-2H+22H^2+3H^3)+\lambda_1^2(4H-3)\left(-2(-1+H(4+H))+\lambda_1^2(4H-1)\right)}{64H^3(2H-1)^3}}\Bigg]^2,
\end{aligned}
\tag{24}
$$

The authors of [23] present their *MSE* equation for (11). They assume there that $\lambda = l + \delta$, where $\delta \in [-0.5, \ 0.5)$, l is an integer part and δ is a fractional part of λ. It is worth noticing that there is no such restriction for δ in the presented method ($|\delta|$ can be greater than 0.5) which affects the estimation results (there are no additional estimation errors for *CiR* = 0.5, 1.5, 2.5, etc. due to a proper choice of k). Moreover, in [6] there was proved that the smallest systematic errors for *CiR* < 2.1 are obtained for $k = 1$ and in [19] – that, due to noise in the signal, $k = 1$ is the best choice for *CiR* less than ca. 1.75–1.99 (the exact value depends on the number of samples N and the noise level). In this case δ is out of the range $[-0.5, \ 0.5)$. The *MSE* equation presented in [23] is:

$$
\begin{aligned}
MSE\left(\hat{\lambda}_1\right) &\cong \sigma_{\lambda_1}^2 \cong \frac{(H^2-\delta^2)^2}{8H^2(2H-1)^2(l+\delta)^2}\frac{ENBW}{SL^2(\delta)}\frac{1}{N\cdot SNR} \\
&\quad \left\{\left[H^2+\delta(\delta+2l)\right]^2+2\left[H-\delta(\delta+2l)\right]^2+2H^3(H-2)+4l^2H^2 \right. \\
&\quad \left. -4\left[H^2-\delta(\delta+2l)\right]\left[H^2-H+\delta(\delta+2l)\right]\rho_1+\left[H^2-(\delta+2l)^2\right](H^2-\delta^2)\rho_2\right\}
\end{aligned}
\tag{25}
$$

and for $l \gg H$:

$$
MSE\left(\hat{\lambda}_1\right) \cong= \frac{(H^2-\sigma^2)^2}{2H^3(2H-1)^3}\frac{ENBW}{SL^2(\sigma)}\frac{1}{N\cdot SNR}(4H-3)\left[(4H-1)\sigma^2+H^2\right]
\tag{26}
$$

where *ENBW* (*Equivalent Noise Band Width*) and $SL(\delta)$ (*Scalloping Loss*) are time window parameters and ρ_1 and ρ_2 are correlation coefficients between spectrum points which can be found in [33].

To compare two *MSE* equations (presented in [21] and in [23]) simulations in Matlab environment were performed. As a variance estimator the *eMSE* (*empirical Mean Square Error*) error was calculated [34]:

$$
eMSE\left(\hat{\lambda}_1\right) = \frac{1}{R}\sum_{j=1}^{R}\left(\hat{\lambda}_j-\lambda_1\right)^2,
\tag{27}
$$

where the number of repetitions R was 10^3. The remaining parameters' values were as in [23]: the value of A_1 was 1, the number of samples $N = 512$, the time window order $H = 2$ (Hanning window), $SNR = 30$ dB and the *CiR* range was $0.1 \leq CiR < 5$. Only the signal phase was not random like in [23] but it was changed in a range from 0 to 2π in steps of 0.01 rad.

To determine the statistical properties of estimators and to compare various estimators, the Cramér-Rao (*CRB*) bound is often used. It sets the lower limit of the estimator's variance – the estimator variance is equal or greater than the *CRB*. It is worth noticing that using the expression for *CRB* in a range *CiR* < 1 (as in [23]) is a rather bad approach because of the presence of the conjugate component in the spectrum and its influence on the estimation (when changing the spectrum shape of the main lobe spectrum) and the *CRB* bound. The *CRB* for many signal cycles observed in the measurement window (for one component in the spectrum) is as follows [34]:

$$CRB\left(\hat{\lambda}_1\right) = \frac{6N}{A_1^2 \pi^2 (N^2 - 1)} \sigma_n^2. \tag{28}$$

For estimation with a small number of cycles (especially for about one cycle) the *MSE* of estimator should be compared with the *CRB* bound, like for a signal spectrum composed of two components (not one). A non-matrix form of this *CRB* was presented in [35] as:

$$CRB\left(\hat{\lambda}_m\right) = \frac{1}{4\pi^2 N \cdot SNR_m} \frac{1}{X_0 + X_C \cos(2(\varphi_2 - \varphi_1)) + X_S \sin(2(\varphi_2 - \varphi_1))}, \tag{29}$$

where $m = 1, 2$ and

$$X_0 = 2K_0 - \frac{K_C^2 + K_S^2}{K_0}, \tag{30}$$

$$X_C = \frac{K_C^2 + K_S^2}{K_0}, \tag{31}$$

$$X_S = -\frac{2K_C K_S}{K_0}. \tag{32}$$

The value of *CRB* depends on the distance between λ_1 and λ_2 (in this case $\lambda_2 = -\lambda_1$ and $\varphi_2 = -\varphi_1$). The values of K_0, K_C and K_S in the (30), (31) and (32) are:

$$K_0 = \frac{\Gamma_2(\Gamma_0^2 - C_0^2 - S_0^2) - \Gamma_0(\Gamma_1^2 + C_1^2 + S_1^2) + 2\Gamma_1(C_0 C_1 + S_0 S_1)}{\Gamma_0^2 - C_0^2 - S_0^2}, \tag{33}$$

$$K_C = \frac{-C_2(\Gamma_0^2 - C_0^2 - S_0^2) - C_0(\Gamma_1^2 + C_1^2 - S_1^2) + 2C_1(\Gamma_0\Gamma_1 - S_0 S_1)}{\Gamma_0^2 - C_0^2 - S_0^2}, \tag{34}$$

$$K_S = \frac{S_2(\Gamma_0^2 - C_0^2 - S_0^2) + S_0(\Gamma_1^2 - C_1^2 + S_1^2) - 2S_1(\Gamma_0\Gamma_1 - C_0 C_1)}{\Gamma_0^2 - C_0^2 - S_0^2}, \tag{35}$$

where

$$\Gamma_r = \frac{1}{N^{r+1}} \sum_{n=n_0}^{n_0+N-1} n^r, \qquad r = 0, 1, 2, \tag{36}$$

$$C_r = \frac{1}{N^{r+1}} \sum_{n=n_0}^{n_0+N-1} n^r \cos(2\pi n(\lambda_1 - \lambda_2)), \qquad r = 0, 1, 2, \tag{37}$$

$$S_r = \frac{1}{N^{r+1}} \sum_{n=n_0}^{n_0+N-1} n^r \sin(2\pi n(\lambda_1 - \lambda_2)), \qquad r = 0, 1, 2. \tag{38}$$

The results of (25) and (26) presented in [23] deviate from the *eMSE* results, especially for *CiR* < 1 (Fig. 1). (25) is more accurate than (26) in this range. For *CiR* > 2 the results of

(25) and (26) are close to each other. The *MSE* equation (24) proposed in this paper is more accurate, especially for *CiR* < 1, where the conjugate component affects most of the results. Using a correction factor (presented in [21]) increases accuracy. The error of calculations of (24) is oscillating in a range of 20% to 40% and for (24) – with the correction factor in a range of up to 20% (oscillating around the *eMSE* value). For (25) and (26) the errors are much bigger for *CiR* < 2. More information about the *MSE* of the proposed method for various values of *H*, *SNR* can be found in [21].
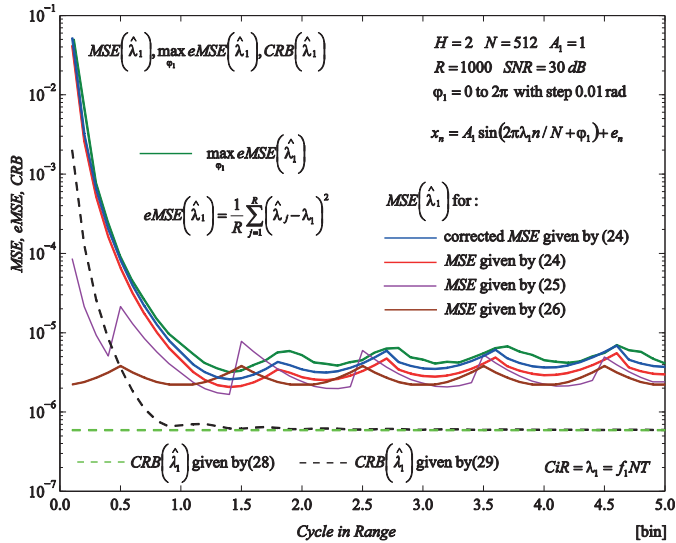
Fig. 1. Statistical properties of the frequency estimator: comparison of four *MSE* expressions in respect of the *CRB* bound for sample measurement parameters.

In practice, harmonic components are often present in the signal. In this case, (10) changes in dependence on the harmonic components which cause bigger estimation errors. For example, for an additional harmonic component *L* (10) is:

$$
X(\lambda) = \frac{A_1}{2j} e^{j\varphi_1} W(\lambda - \lambda_1) - \frac{A_1}{2j} e^{-j\varphi_1} W(\lambda + \lambda_1) +
$$
$$
+ \frac{A_L}{2j} e^{j\varphi_L} W(\lambda - L\lambda_1) - \frac{A_L}{2j} e^{-j\varphi_L} W(\lambda + L\lambda_1). \tag{39}
$$

The general expression for estimation errors caused by the presence of harmonics was presented in 2015 [20] using the MacLaurin approximation. In this paper the whole expression is presented as well as the analytical formulae (see Appendix). The estimation error in this case can be presented as the real part of:

$$
\sum_{L=2}^{M} |\delta_{h,L} f_1| = \sum_{L=2}^{M} \left[\frac{A_L}{A_1} \frac{(-2X_k + X_{k-1} + X_{k+1})z}{(2(-(2+2H-2H^2)X_k + (H-1)^2 X_{k-1} + (H+1)^2 X_{k+1}))} \right], \tag{40}
$$

where *z* is presented in Appendix. In [23] the authors presented the error expression as follows:

$$
\sum_{L=2}^{M} |\delta_{h,L} f_1| = 0.5\lambda^2 \sum_{L=2}^{M} \left(\frac{L^2-1}{2} \frac{A_L}{A_1} \frac{H^2 - \delta^2}{\alpha_L^2 - H^2} \frac{|W(-\alpha_L)|}{|W(-\delta)|} \right)^2, \tag{41}
$$

where $\alpha_L = (L-1)l + L\delta$. To compare these two equations simulations in Matlab were performed for a few cases of H and L (Fig. 2). The results for both equations are similar for a greater value of *CiR* and the fitting accuracy is up to ten times greater than the error value (Fig. 2a). The error values for *CiR* < 2 are greater because of the impact of the conjugate component and some approximations made while determining the expressions (Fig. 2b). However, in this range (40) gives slightly better results.
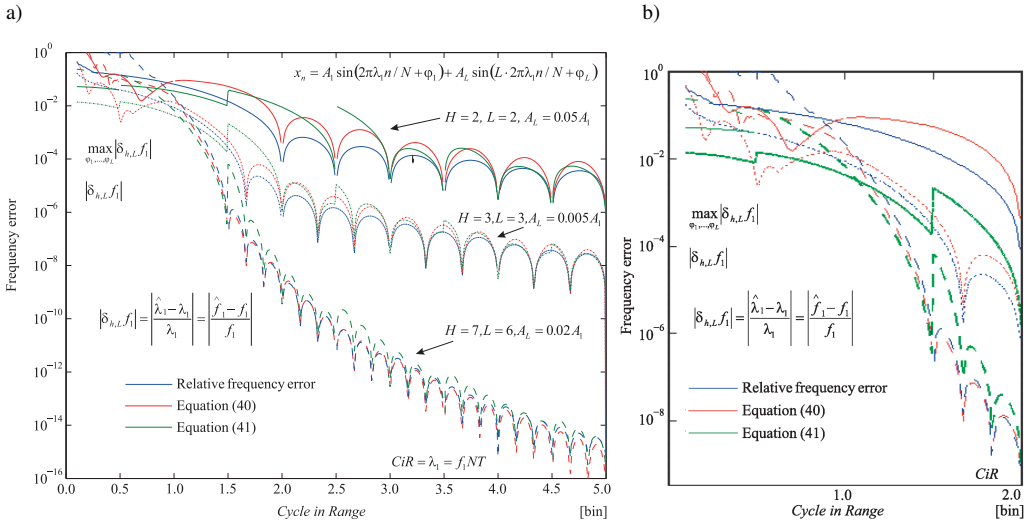
a)   b)

Fig. 2. Frequency-relative estimation errors and two theoretical expressions for $k = 1$ and sample values of H and L: for a range $CiR = 0.1-5$ (a); for a range $CiR = 0.1-2$ (b).

3. Comparison of eight estimation methods

In the conference paper [22] a comparison of several estimation methods was presented. This section extends [22] by comparing more methods, by comparing for a greater value of *CiR* and also by comparing systematic errors of the methods and calculation times of the methods ([22] contained only a comparison for a signal distorted by noise and harmonics).

In this section eight estimation methods (five 3-point IpDFT methods, Prony LS, TLS, ES-PRIT) in respect of accuracy and speed are compared. The tests were performed in Matlab environment for *CiR* < 3 to show how the methods can work when there is only up to three cycles in the measurement window which means *e.g.* 60 ms for the grid signal. The tests were carried out for a signal without disturbances, for a signal distorted by AWGN noise and for a signal distorted by harmonic components. The estimation error values were obtained for each *CiR* value as the maximum in the whole range of components' phases – from 0 to 2π in steps of 0.01 rad. The first method is the one presented in this paper, where the frequency value can be estimated using (11) and (14). The second one is the method from [15], where the frequency estimator for the Hanning window only is:

$$\hat{\lambda}_1 = l + 2\frac{|X_{k+1}| - |X_{k-1}|}{|X_{k-1}| + 2|X_k| + |X_{k+1}|} . \tag{42}$$

The next is the method from [16], where the frequency equation is:

$$\hat{\lambda}_1 = l + \frac{\tan(\pi/N)}{\pi/N} \operatorname{Re}\left\{ \frac{X_{k-1} - X_{k+1}}{-X_{k-1} + 2X_k - X_{k+1}} \right\}. \tag{43}$$

The fourth, IpDFT method is from [17], where:

$$\hat{\lambda}_1 = l + H \frac{|X_{k+1}| - |X_{k-1}|}{|X_{k-1}| + 2|X_k| + |X_{k+1}|} \tag{44}$$

and the last one is the method from [18], where:

$$\hat{\lambda}_1 = l + \frac{2}{\pi} \arctan\left(\frac{X_k}{2} \left(\frac{1}{X_{k-1}} - \frac{1}{X_{k+1}} \right) \Big/ \cos\left(\frac{\pi}{2N} \right) \right). \tag{45}$$

The Prony LS, TLS and ESPRIT methods were chosen for comparison with the IpDFT methods. Prony's methods have been very popular in the recent years in many applications because of their universality and possibility to calculate damped ratios for signal components. The ESPRIT method is one of the subspace methods and it is based on the properties of autocorrelation matrices. The TLS method is a development of the LS methods and gives more accurate results because in the linear matrix equation it takes into consideration distortions of two matrices.

3.1. Accuracy for pure signal

In the first part of tests the estimation results were obtained for a sine-wave signal (1) for $L = M = 1$ without any disturbances. The systematic errors were calculated as relative errors for: $H = 2, 3, \ldots, 7$; $N = 32$ and 64. In the tested range of $CiR < 3$ the parametric methods are more accurate than IpDFT methods (Fig. 3). The systematic error of the proposed method
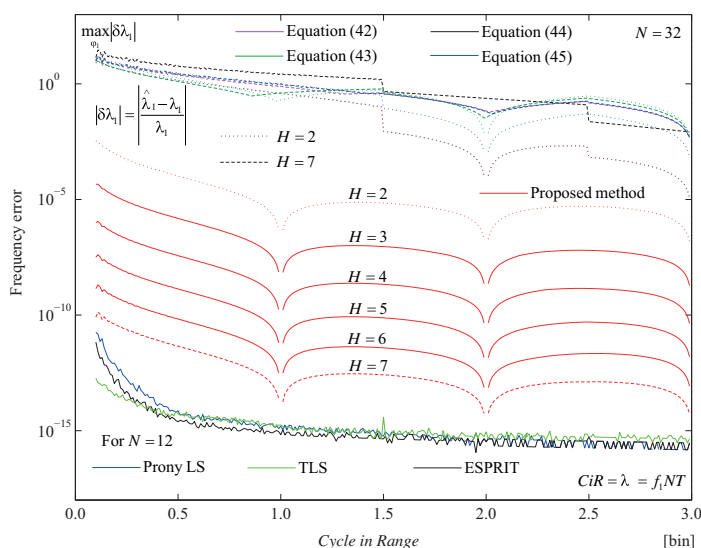

Fig. 3. Systematic errors of estimation methods for $H = 2, \ldots, 7$ and $N = 32$ as functions of *CiR*.

293

decreases when the H value increases, *e.g.* the error values are approximately 10^{-5} for $H = 2$ and 10^{-12} for $H = 7$ for $CiR = 1.5$ and $N = 32$ (Fig. 3, Fig. 4). However, for other IpDFT methods this causes bigger errors. An increase in N value also decreases error values for the proposed method (Fig. 4) – the systematic errors are inversely proportional to N^{2H} [6]. *E.g.*, for $N = 64$ and $H = 6$ or 7 the estimation error values are at the same level as for the parametric methods. A greater value of N causes faster reaching this level. Moreover, the error values for the proposed method are much smaller (several orders) than for other IpDFT methods (Fig. 4).
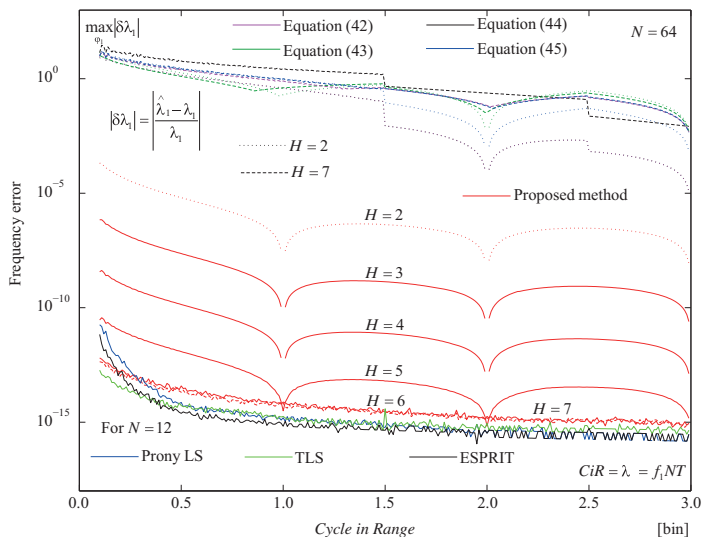

Fig. 4. Systematic errors of estimation methods for $H = 2, \ldots, 7$ and $N = 64$ as functions of *CiR*.

Very accurate results can be obtained for the parametric methods even for a small value of N, *e.g.* 12, and it does not have to be a value that is a power of 2, like for FFT-based methods. It is worth noticing that the model order for parametric methods has to be chosen before estimation. An increase in the *CiR* value increases accuracy of all methods.

3.2. Accuracy for signal distorted by harmonics

The second part of tests was dedicated to estimation for a signal distorted by harmonic components. Such a situation occurs very often in real-time measurements. To the signal there were added the 2nd, 3rd and 4th harmonics with the same amplitude $A_L = A_1/100$ which fits the ranges present in the EN 50160 norm for the grid signal [36]. Phases of components were changed in a range from 0 to 2π in steps of 0.01 rad. Usually, harmonics with a small number L affect most of the estimation results and that is why these components were taken into consideration despite the fact that they have a small impact on THD of the grid signal. The error values were calculated for $H = 2$ and $H = 7$. The results show that the parametric methods are much more accurate than IpDFT methods for $H = 2$ and $H = 7$ (from approximately 10^{10} to 10^{14} times for $H = 2$ and from approximately 10^{12} to 10^{15} times for $H = 7$ and $CiR = 1.5$) (Fig. 5, Fig. 6). However, the

error value increases for *CiR* below 1 and for *CiR* = 0.1 it reaches error values of the proposed method.
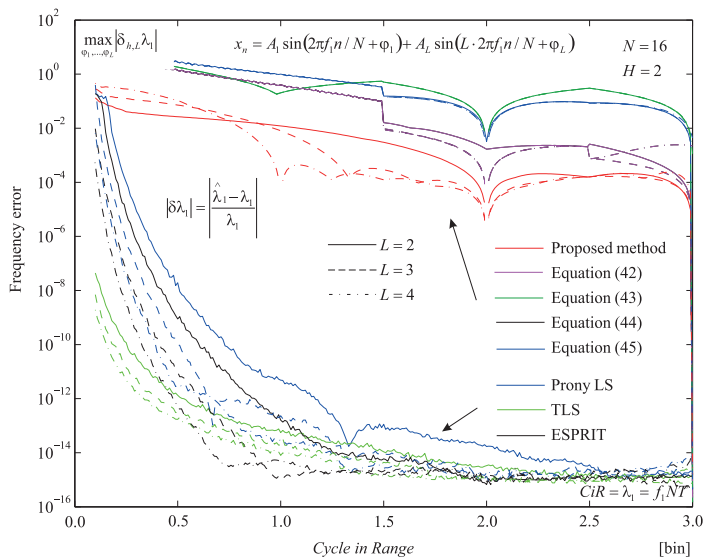

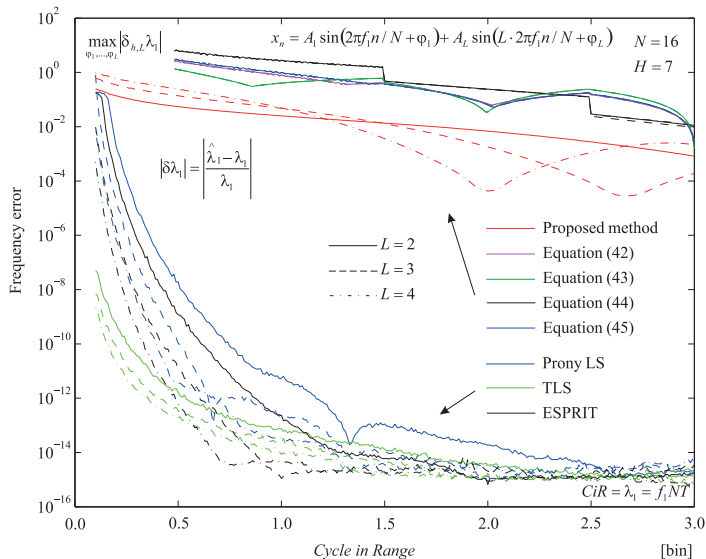Fig. 5. The effect of harmonic components on estimation results for eight estimation methods and *H* = 2.

Fig. 6. The effect of harmonic components on estimation results for eight estimation methods and *H* = 7.

The IpDFT methods are very sensitive to the presence of harmonics because they are based on the signal spectrum. Two basic approaches to changing this situation are: removing/reducing

harmonics in the spectrum or taking them into consideration while obtaining analytical forms of estimators. The proposed method is still more accurate than other IpDFT methods – the error level is approximately from 10^{-4} to 10^{-2} for $H = 2$ and approximately 10^{-1} for $H = 7$ and $CiR = 1$. The expression that enables to obtain the theoretical estimation error value for a signal with harmonics is presented in Section 2.

3.3. Accuracy for signal distorted by AWGN noise

In this part the results obtained for the signal distorted by AWGN noise (under the assumption that the square of systematic errors is negligible relative to the estimator variance) are presented. The *SNR* value was changed in a range 30 dB–90 dB to show performance of methods for a poor signal (*i.e.* disturbed by noise with a high level of variance) and a "noise-free" signal (in practical cases assumed for $SNR \geq 90$ dB). Moreover, this range includes a typical range for the grid signal (approximately 40 dB–60 dB) for which the proposed method was originally developed. Other measurement parameters were: $H = 2$, the number of repetitions $R = 1000$, $CiR = 1.3$, $N = 8$, 32 and 512. (27) was used as the variance estimator. As previously, the parametric methods can be used for a small value of N and they give very accurate results. Error values of these methods and the proposed method decrease when the *SNR* value increases (the signal is less distorted by noise) (Fig. 7). For example, the square root of the *eMSE* error is approximately 2×10^{-3} bin for $SNR = 30$ dB and approximately 10^{-6} bin for $SNR = 90$ dB. Estimation results of other IpDFT methods are very poor. The *eMSE* error values with reference to the *CRB* bound are approximately 1.6–1.85 for the parametric methods (for $N = 8$) and about 2.35 for the proposed method (Fig. 8). An increase of the N value increases accuracy of the proposed method but does not decrease the relation to the *CRB* bound (unless the level of systematic error is higher than the error caused by noise). The expression that enables to obtain the estimation error value before the estimation process for a signal with noise is presented in Section 2.
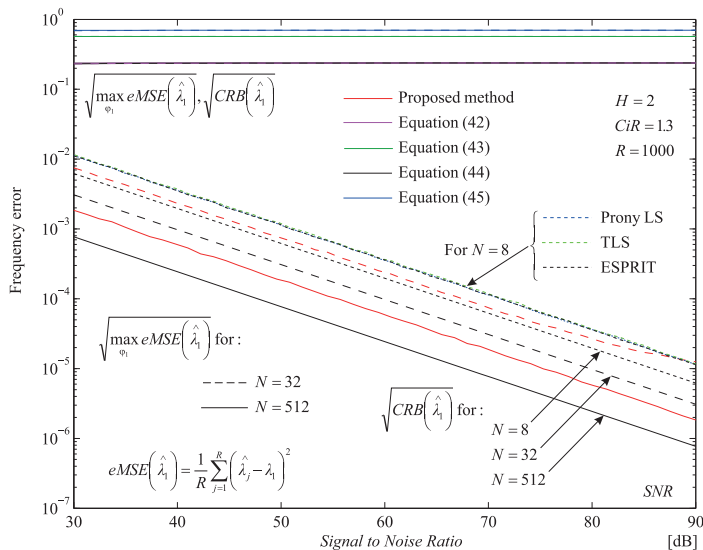

Fig. 7. Statistical properties of the estimation methods: the root-square *eMSE* error and the reference to the Cramér-Rao bound as functions of *SNR*.
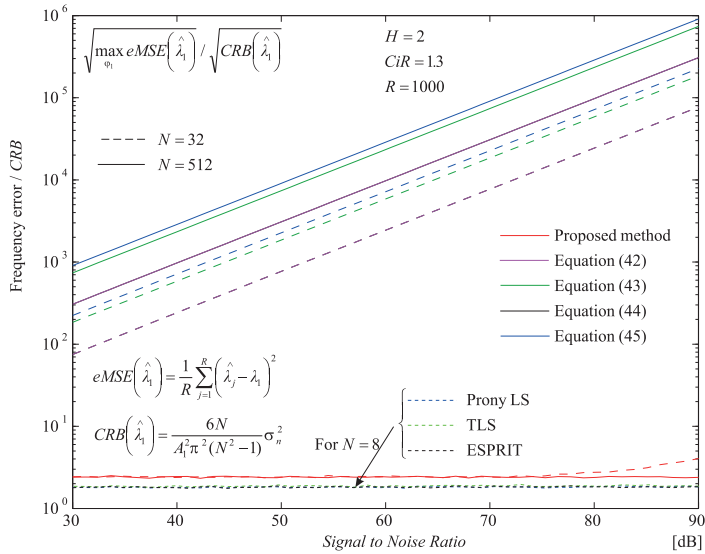
Fig. 8. Statistical properties of the estimation methods with reference to the Cramér-Rao bound as functions of *SNR*.

3.4. Calculation speed of methods

There can be distinguished two speed parameters for the estimation methods: the estimation time which denotes duration of the whole estimation procedure (the time of observed cycles and the calculation time of methods) and the calculation time of methods after the acquisition of signal samples. Greater values of *N* in the measurement window affect positively the estimation
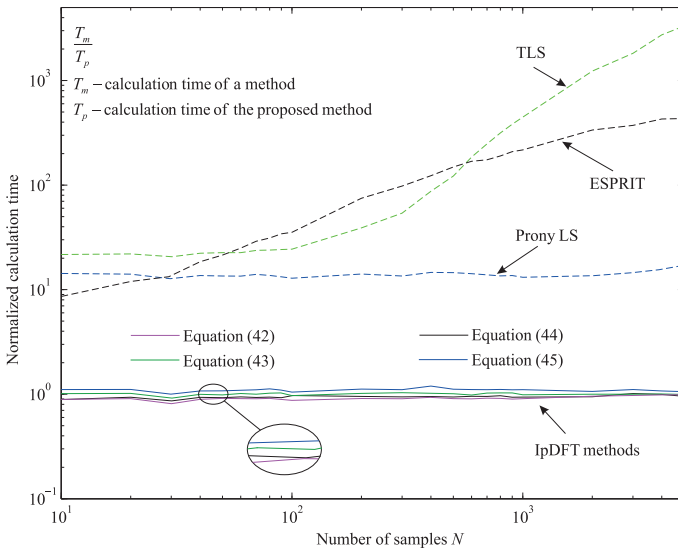

Fig. 9. Normalized calculation times of the estimation methods in respect of the calculation time of the proposed method as functions of *N*.

results. However, a greater N means also a longer calculation time of a method. In this part the tests were dedicated to evaluating calculation times of the estimation methods using tic/toc commands and an average of 1000 repetitions. The parametric methods are slower than IpDFT methods from approximately 10–30 for $N = 10$ to approximately 20–3000 times for $N = 5000$ (Fig. 9). Calculation times for all IpDFT methods are similar because they are based on the Fast Fourier Transform procedure (with the computational complexity $N \log_2 N$) and additional calculations times are significantly shorter than the FFT execution time. The longer time here means that calculations of the spectrum are based on a greater value of N (Fig. 10).
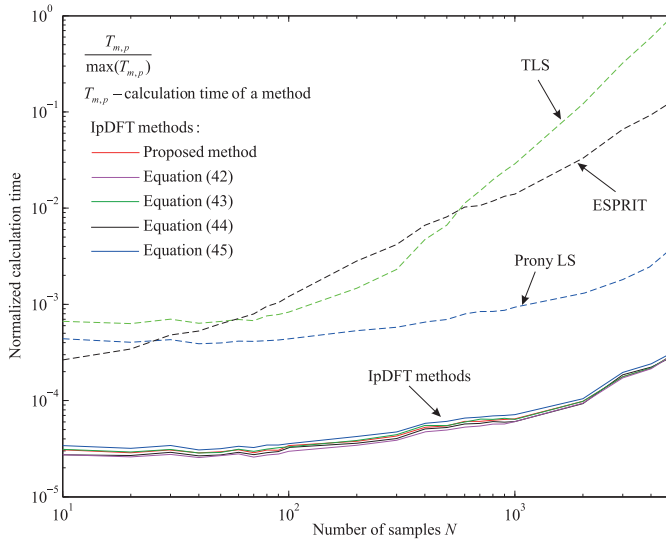

Fig. 10. Normalized calculation times of the estimation methods in respect of the maximum calculation time obtained in tests as functions of N.

4. Conclusions

The paper consists of two main parts. The first part is dedicated to the response to the paper [23], where the authors compare their method with the method presented in [6] and give formulae to calculate the MSE error and the error for a sine-wave signal distorted by harmonics. In the papers [20, 21] such formulae were also presented. After the comparison included in Section 2 it can be concluded that they are at least as accurate as the expressions from [23] or even more for $CiR < 1$.

The second part of the paper is dedicated to comparison of eight estimation methods in respect of their accuracy and speed. They are divided into two main groups: parametric methods (TLS, Prony LS, ESPRIT) and nonparametric methods (five 3-point IpDFT methods including the method presented in this paper). The tested sine-wave signal was analysed as: a pure sinusoidal signal, a signal distorted by noise and a signal distorted by harmonics. Moreover, the methods were tested for various numbers of samples N in the measurement window to compare their calculation times. Generally speaking, the parametric methods are more accurate than IpDFT methods for various measurement conditions. The biggest difference between errors is for the signal distorted by harmonics. The parametric methods can give accurate results even for a small value of N and for a very small value of CiR (below 0.5). However, due to their complexity they

are much slower than IpDFT methods (even 3000 times for $N = 5000$), what can cause problems in real-time systems. The proposed IpDFT method is more accurate than other IpDFT methods and its accuracy can be adjusted using various values of H and N. It takes into account the conjugate component in the signal spectrum and can give accurate results even for *CiR* <1. The level of systematic errors is approximately 10^{-5} for $N = 64$, $H = 2$ and *CiR* = 1.3; the level of errors caused by the presence of harmonics is approximately 10^{-4} for the fourth harmonic, $H = 2$, *CiR* = 1.3 and $N = 16$; the level of errors caused by the presence of noise is approximately 10^{-4} bin for *SNR* = 60 dB, $H = 2$, $N = 512$ and *CiR* = 1.3. Additionally, the method is based on the FFT transform and it is very fast which predisposes it to real-time applications. In this sense it is a universal method which is very easy to implement and adjust to current measurement conditions. Other IpDFT methods can be also used in real-time systems but only for the *CiR* value greater than two or even more in dependence on the measurement parameters. The parametric methods are used in applications where accuracy is more important than complexity or calculation time, or where the hardware parameters are good enough to make necessary calculations in a short time.

Acknowledgements

References

[1] Kelley, K., Light, R.P., Agarwal R. (2007). Trended cosinor change model for analyzing hemodynamic rhythm patterns in hemodialysis patients. *Hypertension*, 50(1), 143–150.

[2] Engels, F., Heidenreich, P., Zoubir, A.M., Jondral, F.K., Wintermantel, M. (2017). Advances in Automotive Radar: A framework on computationally efficient high-resolution frequency estimation. *IEEE Signal Processing Magazine*, 34(2), 36–46.

[3] Blaira, J.J., Linnenbrinkb, T.E. (2003). Corrected rms error and effective number of bits for sine wave ADC tests. *Computer Standards and Interfaces*, 26(1), 43–49.

[4] Powell, K. (2011). Estimating the impact of structural vibration on adaptive optics system performance. *Journal of Applied Optics*, 50, 2185–2191.

[5] Li, X., Zhang, Y., Amin, M.G. (2009). Multifrequency-based range estimation of RFID Tags. *IEEE International Conference on RFID*, 147–154.

[6] Borkowski, J., Kania, D., Mroczka, J. (2014). Interpolated DFT-based Fast and Accurate Frequency Estimation for the Control of Power. *IEEE Transactions on Industrial Electronics*, 61(12), 7026–7034.

[7] Abbas, S.A., Sun, Q., Foroosh, H. (2016). Frequency estimation of sinusoids from nonuniform samples. *Signal Processing*, 129, 67–81.

[8] Zygarlicki, J., Mroczka, J. (2012). Variable-frequency Prony method in theanalysis of electrical power quality. *Metrol. Meas. Syst.*, 19(1), 39–48.

[9] Zygarlicki, J., Mroczka, J. (2012). Prony's method used for testing harmonics and interharmonics in electrical power systems. *Metrol. Meas. Syst.*, 19(4), 659–672.

[10] Ahmad, A., Schlindwein, F.S., Ng, G.A. (2010). Comparison of computation time for estimation of dominant frequency of atrial electrograms: Fast fourier transform, blackman tukey, autoregressive and multiple signal classification. *Journal Biomedical Science and Engineering*, 3, 843–847.

[11] Chen, H., Hou, C., Zhu, W.P., Liu, W., Dong, Y.Y., Peng, Z. (2017). ESPRIT-like two dimensional direction finding for mixed circular and strictly noncircular sources based on joint diagonalization. *Signal Processing*, 141, 48–56.

[12] Wang, M., Nehorai, A. (2017). Coarrays, MUSIC, and the Cramér-Rao Bound. *IEEE Transactions on Signal Processing*, 65(4), 933–946.

[13] Koglin, H.-J, Leonowicz, Z., Lobos, T. (2006). High-Resolution Spectrum Estimation Methods for Signal Analysis in Power Systems. *IEEE Transactions on Instrumentation and Measurement*, 55(1), 219–225.

[14] Huckle, T. (1998). Computations with Gohberg-Semencul-type formulas for Toeplitz matrices. *Linear Algebra and its Applications*, 273(1), 169–198.

[15] Agrež, D. (2002). Frequency Estimation of the Non-Stationary Signals Using Interpolated DFT. *IEEE Instrumentation and Measurement Technology Conference*, 2, 925–930.

[16] Candan, C. (2013). Analysis and Further Improvement of Fine Resolution Frequency Estimation Method From Three DFT Samples. *IEEE Signal Processing Letters*, 20(9), 913–916.

[17] Belega, D., Dallet, D., Eynard, G. (2010). Influence of the Noise on the Amplitude Estimation of a Sive-Wave by the Three-Point Interpolated DFT Method. *4th International Symposium on Communications, Control and Signal Processing*, 1–5.

[18] Liang, X., Liu, S., Pan, X., Zhang, Q., Chen, F. (2016). A New and Accurate Estimator With Analytical Expression for Frequency Estimation. *IEEE Communications Letters*, 20(1), 105–108.

[19] Borkowski, J., Kania, D., Mroczka, J. (2014). Influence of A/D Quantization in Interpolated-DFT-Based System of Power Control with Small Delay. *Metrol. Meas. Syst.*, 2(3), 423–432.

[20] Kania, D. (2015). Estimation of the sinusoidal oscillation parameters in the adaptive optics system based on the example of the photovoltaic system. *SPIE Optics and Optoelectronics Conference*, 1–8.

[21] Kania, D., Borkowski, J. (2016). Influence of noise on the IpDFT-based estimation of the grid frequency in Renewable Energy Systems. *IEEE International Conference on Environment and Electrical Enegineering*, 1–5.

[22] Kania, D., Borkowski, J. (2017). Estimation methods of multifrequency signals with noise and harmonics for PV systems with a DSP processor. *IEEE International Conference on Telecommunications and Signal Processing*, 1–4.

[23] Belega, D., Petri, D. (2017). Effect of noise and harmonics on sine-wave frequency estimation by interpolated DFT algorithms based on few observed cycles. *Signal Processing*, 140, 207–218.

[24] Wang, Y., Wei, W., Xiang, J. (2017). Multipoint interpolated DFT for sine waves in short records with DC components. *Signal Processing*, 131, 161–170.

[25] Lee, M., Clarke, D. (2005). A Frequency Estimation Comparison between the Modified Covariance Method and the Fourier Transform. *World Scientific and Engineering Academy and Society Conference*, 1–4.

[26] Almoosawy, A.N., Hussain, Z.M., Murad, F.A. (2014). Frequency Estimation of Single-Tone Sinusoids Under Additive and Phase Noise. *International Journal of Advanced Computer Science and Applications*, 5(9), 102–106.

[27] Costa, F.F., Fernandes, D.A., de Almeida, L.A.L., Naidu, S.R. (2005). Prony's method versus FFT for analyzing power converters signals. *European Conference on Power Electronics and Applications*, 1–9.

[28] Nuttall, A.H. (1981). Some Windows with Very Good Sidelobe Behavior. *IEEE Transactions on Acoustics, Speech, and Signal Processing*, 29(1), 84–91.

[29] Rife, D.C., Vincent, G.A. (1970). Use of the Discrete Fourier Transform in the Measurement of Frequencies and Levels of Tones. *Bell System Technical Journal*, 49, 197–228.

[30] Belega, D., Dallet, D. (2009). Multifrequency signal analysis by Interpolated DFT method with maximum sidelobe decay windows. *Measurement*, 42(3), 420–426.

[31] Belega, D. (2005). The maximum sidelobe decay windows. *Revue Roumaine des Sciences Techniques. Série Electrotechnique et Energetique*, 3, 349–356.

[32] Chen, K.F., Cao, X., Li, Y.F. (2009). Sine wave fitting to short records initialized with the frequency retrieved from Hanning windowed FFT spectrum. *Measurement*, 42(1), 127–135.

[33] Belega, D., Dallet, D. (2009). Multifrequency signal analysis by Interpolated DFT method with maximum sidelobe decay windows. *Measurement*, 42, 420–426.

[34] Handel, P. (2000). Properties of the IEEE-STD-1057 four-parameter sine wave fit algorithm. *IEEE Transactions on Instrumentation and Measurement*, 49(6), 1189–1193.

[35] Dilaveroğlu, E. (1998). Nonmatrix Cramér-Rao Bound Expressions for High Resolution Frequency Estimators. *IEEE Transactions on Signal Processing*, 46(2), 463–474.

[36] Voltage Characteristics in Public Distribution Systems (2010), EN 50160.

Appendix

Derivation of expression (40)

The spectrum expression for a signal with a harmonic component L can be presented in respect of the A_1 value as the sum of two components: one independent and one dependent on $x = A_L/A_1$:

$$\frac{X(\lambda)}{A_1} = a_0 + \frac{A_L}{A_1} a_1 . \tag{A.1}$$

In this case the expression for (14) takes the form:

$$\hat{\lambda}_1 = \mathrm{Re}\left\{ \sqrt{\frac{a+bx}{c+dx}} \right\}, \tag{A.2}$$

where

$$a = -X_{k-1}(H-1)^2 + X_k(-2H^2 + 2H + 2) - X_{k+1}(H+1)^2, \tag{A.3}$$

$$
\begin{aligned}
b = \sum_{L=2}^{M} x & \left[\frac{2^{-2H} e^{j(\varphi_L - \varphi_1 + L\lambda\pi)}}{\pi(1-L\lambda) \prod_{h=1}^{H} \left(h^2 - (1-L\lambda)^2 \right)} \cdot N\left((-2 - 2H + 2H^2) X_k + \frac{(H-1)^2(H-L\lambda)}{-1+H+L\lambda} X_{k-1} + \right. \right. \\
& \left. + \frac{(H+1)^2(-2+H+L\lambda)}{1+H-L\lambda} X_{k+1} \right) (2H-2)! \mathrm{Sin}(L\lambda\pi) \\
& - \frac{2^{-2H} e^{j(-\varphi_L - \varphi_1 - L\lambda\pi)}}{\pi(1+L\lambda) \prod_{h=1}^{H} \left(h^2 - (1+L\lambda)^2 \right)} \cdot N\left((2+2H-2H^2) X_k - \frac{(H-1)^2(H-L\lambda)}{-1+H+L\lambda} X_{k-1} \right. \\
& \left. \left. - \frac{(H+1)^2(-2+H+L\lambda)}{1+H-L\lambda} X_{k+1} \right) (-2H+2)! \mathrm{Sin}(L\lambda\pi) \right],
\end{aligned}
\tag{A.4}
$$

$$c = X_{k-1} - 2X_k + X_{k+1}, \tag{A.5}$$

$$d = \sum_{L=2}^{M} x \left[\frac{2^{-2H} e^{j(\varphi_L - \varphi_1 + L\lambda\pi)} N \left(2X_k + \frac{H - L\lambda}{-1 + H + L\lambda} X_{k-1} + \frac{-2 + H + L\lambda}{1 + H - L\lambda} X_{k+1} \right) (2H-2)! \operatorname{Sin}(L\lambda\pi)}{\pi(1-L\lambda) \prod_{h=1}^{H} \left(h^2 - (1-L\lambda)^2 \right)} \right.$$
$$\left. - \frac{2^{-2H} e^{j(-\varphi_L - \varphi_1 - L\lambda\pi)} N \left(-2X_k - \frac{H + L\lambda}{-1 + H + L\lambda} X_{k-1} - \frac{-2 + H - L\lambda}{1 + H + L\lambda} X_{k+1} \right) (2H-2)! \operatorname{Sin}(L\lambda\pi)}{\pi(1+L\lambda) \prod_{h=1}^{H} \left(h^2 - (1+L\lambda)^2 \right)} \right]. \tag{A.6}$$

Using the MacLaurin expansion of (A.2) in respect of x variable it can be obtained:

$$\hat{\lambda}_1 = \operatorname{Re} \left\{ \sqrt{\frac{-X_{k-1}(H-1)^2 + X_k(-2H^2 + 2H + 2) - X_{k+1}(H+1)^2}{X_{k-1} - 2X_k + X_{k+1}}} (1 + \varepsilon) \right\}, \tag{A.7}$$

where ε is zero when there is no harmonic components in the signal. Taking into consideration after many simulations and practical tests that the relative systematic error is much below 1 (*i.e.* 100%) and also the value of ε is below 1 there can be assumed:

$$\left| \frac{\hat{\lambda}_1(1 + \varepsilon) - \lambda_1}{\lambda_1} \right| \approx \left| \frac{\hat{\lambda}_1 - \lambda_1}{\lambda_1} + \varepsilon \right| = |\delta\lambda_1| + |\varepsilon|. \tag{A.8}$$

After some algebraic transformations the ε value for a signal with harmonics is presented as follows:

$$\varepsilon = \sum_{L=2}^{M} \frac{A_L}{A_1} \frac{-2X_k + X_{k-1} + X_{k+1}}{\left(2 \left(-(2 + 2H - 2H^2)X_k + (H-1)^2 X_{k-1} + (H+1)^2 X_{k+1} \right) \right)} z, \tag{A.9}$$

where

$$z \approx -\frac{\left(-(2 + 2H - 2H^2)X_k + (H-1)^2 X_{k-1} + (H+1)^2 X_{k+1} \right) 2^{-2H} \sqrt{N}}{(-2X_k + X_{k-1} + X_{k+1})^2}$$

$$\cdot \left[\frac{\left(2X_k + \frac{H - L\lambda}{-1 + H + L\lambda} X_{k-1} + \frac{-2 + H + L\lambda}{1 + H - L\lambda} X_{k+1} \right) (2H-2)! \operatorname{Sin}(L\lambda\pi)}{\pi(1-L\lambda) \prod_{h=1}^{H-1} \left(h^2 - (1-L\lambda)^2 \right)} \right.$$

$$\left. - \frac{\left(-2X_k - \frac{H + L\lambda}{-1 + H + L\lambda} X_{k-1} - \frac{-2 + H - L\lambda}{1 + H + L\lambda} X_{k+1} \right) (2H-2)! \operatorname{Sin}(L\lambda\pi)}{\pi(1+L\lambda) \prod_{h=1}^{H-1} \left(h^2 - (1+L\lambda)^2 \right)} \right] + \frac{2^{-2H} \sqrt{N}}{(-2X_k + X_{k-1} + X_{k+1})}$$

$$\cdot \left[-\frac{\left((-2 - 2H + 2H^2)X_k + \frac{(H-1)^2(H-L\lambda)}{-1 + H + L\lambda} X_{k-1} + \frac{(H+1)^2(-2 + H + L\lambda)}{1 + H - L\lambda} X_{k+1} \right) (2H-2)! \operatorname{Sin}(L\lambda\pi)}{\pi(1-L\lambda) \prod_{h=1}^{H-1} \left(h^2 - (1-L\lambda)^2 \right)} \right.$$

$$\left. + \frac{\left((2 + 2H - 2H^2)X_k - \frac{(H-1)^2(H-L\lambda)}{-1 + H + L\lambda} X_{k-1} - \frac{(H+1)^2(-2 + H + L\lambda)}{1 + H - L\lambda} X_{k+1} \right) (-2H+2)! \operatorname{Sin}(L\lambda\pi)}{\pi(1+L\lambda) \prod_{h=1}^{H-1} \left(h^2 - (1+L\lambda)^2 \right)} \right]. \tag{A.10}$$